ICSV13 - Vienna
The Thirteenth International Congress on Sound and Vibration
Vienna, Austria, July 2-6, 2006

HYBRID MUFFLERS WITH SHORT LATERAL CHAMBERS: ANALYTICAL, NUMERICAL AND EXPERIMENTAL STUDIES

F. D. Denia*[1], A. Selamet[2], M. J. Martínez[1] and A. J. Torregrosa[3]

[1]Departamento de Ingeniería Mecánica y de Materiales, Universidad Politécnica de Valencia
Camino de Vera s/n, 46022 Valencia, Spain
[2]Department of Mechanical Engineering and The Center for Automotive Research
The Ohio State University, Columbus, Ohio 43210, USA
[3]CMT-Motores Térmicos, Universidad Politécnica de Valencia
Camino de Vera s/n, 46022 Valencia, Spain
fradegu1@mcm.upv.es

Abstract

An analytical model is presented for the acoustic attenuation performance analysis of circular hybrid mufflers consisting of two short lateral chambers and a central dissipative cavity filled with sound absorbing material. The two-dimensional axisymmetric analytical approach developed to evaluate the muffler performance is based on an eigenequation that accounts for the wave propagation through the absorbing material and the perforations. Once the solution of the transversal eigenproblem is computed, the muffler transmission loss is calculated by matching the acoustic pressure and normal velocity across each geometrical discontinuity. The validation of the proposed procedure is carried out by means of the finite element method and some experimental measurements. The sound attenuation is examined and compared considering the effect of the internal geometry of the muffler, the properties of the sound absorbing material and the porosity of the perforated central pipe. It is shown that the combination of the radial resonances in the short lateral chambers and the dissipative effects associated with the central cavity can lead to an improved acoustic performance in a wide frequency range.

INTRODUCTION

The acoustic behaviour of short expansion chambers has been studied in several works [3, 10, 11, 13], showing that a strong attenuation resonant peak can be obtained at a frequency that depends on the internal geometry of the chamber. The transversal waves dominate the acoustic field in these short configurations, and therefore very little similarity is found between one-dimensional and multidimensional predictions

[11], thus justifying the consideration of the latter for design purposes. On the other hand, dissipative silencers have been shown to be suitable for controlling noise in automotive exhaust systems since broadband attenuation performance is obtained [1, 9], mainly in the mid and high frequency range. To reduce the computational requirements, the development of analytical and semi-analytical modelling procedures is found to be a general trend [6, 7, 14], rather than using full numerical schemes.

Some recent works have demonstrated the benefit of combining both types of behaviour in hybrid mufflers, that is, reactive and dissipative effects for low and high frequencies respectively, which may lead to a broadband attenuation performance including resonant peaks at particular frequencies that can be previously selected by the designer. In the work of Selamet *et al.* [12], a hybrid silencer combining a Helmholtz resonator and two dissipative chambers was studied by means of the boundary element method (BEM). In reference [5], the acoustic behaviour of a hybrid muffler combining a concentric folded resonator and a dissipative chamber is studied by BEM. The work of Denia *et al.* [4] analyses the sound attenuation of partially-filled perforated dissipative circular mufflers with extended inlet/outlet. The effect of the extended lengths as well as fiber resistivity is studied, showing that it is possible to take advantage of the resonant behaviour of the extensions at low and mid frequencies and to retain partially the good properties of the dissipative mufflers at higher frequencies.

The objective of the present work is to investigate the acoustic performance of circular hybrid mufflers consisting of two short lateral chambers and a central dissipative cavity filled with sound absorbing material. This hybrid configuration exhibits an attenuation that combines the effect of transversal resonances in the lateral chambers, leading to a high noise attenuation level at selected frequencies, and dissipation in the absorbing material, providing a suppression of high frequency noise. Therefore an improved acoustic performance can be obtained with a suitable selection of the geometrical parameters involved. An axisymmetric analytical approach is presented, which shows good agreement in comparison with finite element calculations and experimental measurements for some selected configurations. A number of geometries are studied, analysing the effect of the muffler geometry, the perforated pipe and the fiber resistivity.

MATHEMATICAL MODEL

Figure 1 shows the geometry of a hybrid muffler consisting of two lateral chambers and a central perforated dissipative chamber. Seven regions denoted by A, B, C, D (including both the central passage and outer cavity filled with sound absorbing material), E, F and G are considered. The total length L of the hybrid muffler is divided into two lateral chambers with lengths L_B and L_D, a central dissipative chamber with length L_C and two separation rigid plates with thickness t_{p1} and t_{p2}. For the central chamber, the nondimensionalized acoustic impedance of the perforated passage is given by $\tilde{\zeta}_p$ [14] and the absorbing material of the outer cavity is assumed to be homogeneous and isotropic, characterized by the complex speed of sound $\tilde{c}$

and density $\tilde{\rho}$ [2]. The air in the lateral chambers and the passage is characterized by the speed of sound c_0 and density ρ_0.

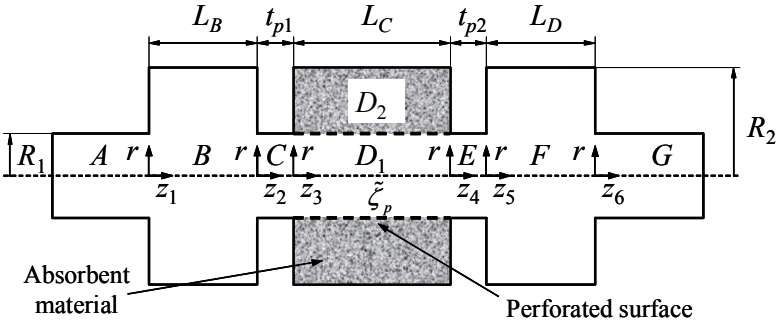

Figure 1 – Hybrid muffler with lateral chambers and central perforated dissipative chamber

The solution of the governing wave equation may be expressed for region A (and B, C, E, F and G) as [8]

$$P_A(r,z_1)=\sum_{n=0}^{\infty}\left(A_n^+ \mathrm{e}^{-\mathrm{j}k_{z,A,n}z_1}+A_n^- \mathrm{e}^{\mathrm{j}k_{z,A,n}z_1}\right)\psi_{A,n}(r) \tag{1}$$

with $\mathrm{j}=\sqrt{-1}$ being the imaginary unit, n the mode number, (r, z_1) the cylindrical co-ordinates, A_n^+ and A_n^- the wave coefficients, $\psi_{A,n}(r)$ the eigenfunction (given by $\mathrm{J}_0(k_{r,A,n}r)$, the zeroth order Bessel function of the first kind), and $k_{r,A,n}$ the radial wavenumber satisfying the rigid wall boundary condition. The axial wavenumber $k_{z,A,n}$ of the mode n is given by $k_{z,A,n}^2=k_0^2-k_{r,A,n}^2$, with $k_0=\omega/c_0$ being the wavenumber in air and ω the angular frequency.

The acoustic velocity in z direction may be written, from Equation (1) and the linearized momentum equation [8], as

$$U_A(r,z_1)=\frac{1}{\rho_0\,\omega}\sum_{n=0}^{\infty}k_{z,A,n}\left(A_n^+ \mathrm{e}^{-\mathrm{j}k_{z,A,n}z_1}-A_n^- \mathrm{e}^{\mathrm{j}k_{z,A,n}z_1}\right)\psi_{A,n}(r) \tag{2}$$

In region D, the acoustic pressure is written as

$$P_D(r,z_3)=\sum_{n=0}^{\infty}\left(D_n^+ \mathrm{e}^{-\mathrm{j}k_{z,D,n}z_3}+D_n^- \mathrm{e}^{\mathrm{j}k_{z,D,n}z_3}\right)\psi_{D,n,P}(r) \tag{3}$$

where the transversal pressure eigenfunction is given by

$$\psi_{D,n,P}(r)=\psi_{D_1,n,P}(r)\quad 0\le r\le R_1 \qquad \psi_{D,n,P}(r)=\psi_{D_2,n,P}(r)\quad R_1\le r\le R_2 \tag{4}$$

The axial velocity can be expressed as

$$U_D(r,z_3)=\frac{1}{\rho_0\,\omega}\sum_{n=0}^{\infty}k_{z,D,n}\left(D_n^+ \mathrm{e}^{-\mathrm{j}k_{z,D,n}z_3}-D_n^- \mathrm{e}^{\mathrm{j}k_{z,D,n}z_3}\right)\psi_{D,n,U}(r) \tag{5}$$

where the transversal velocity eigenfunction $\psi_{D,n,U}(r)$ is obtained from $\psi_{D,n,P}(r)$ by multiplying by $\rho_0/\tilde{\rho}$ for $R_1\le r\le R_2$.

The axial wavenumber in the central inner duct and outer chamber with absorbing material, denoted by $k_{z,D,n}$, is related to the radial wavenumber of the air $k_{r,D,n}$ and fiber $\tilde{k}_{r,D,n}$ by means of

$$k_{z,D,n}^2 = k_0^2 - k_{r,D,n}^2 \qquad k_{z,D,n}^2 = \tilde{k}^2 - \tilde{k}_{r,D,n}^2 \tag{6}$$

The calculation of the wavenumbers as well as the eigenfunctions can be carried out by means of the procedure shown in the work [14]. The following eigenequation is obtained

$$\frac{\rho_0 \tilde{k}_{r,D,n}}{\tilde{\rho} k_{r,D,n}} \left(\frac{\mathrm{J}_0\left(k_{r,D,n} R_1\right)}{\mathrm{J}_1\left(k_{r,D,n} R_1\right)} + \frac{\mathrm{j}\tilde{\zeta}_p k_{r,D,n}}{k_0} \right) = \frac{\mathrm{J}_0\left(\tilde{k}_{r,D,n} R_1\right)\mathrm{Y}_1\left(\tilde{k}_{r,D,n} R_2\right) - \mathrm{Y}_0\left(\tilde{k}_{r,D,n} R_1\right)\mathrm{J}_1\left(\tilde{k}_{r,D,n} R_2\right)}{\mathrm{J}_1\left(\tilde{k}_{r,D,n} R_1\right)\mathrm{Y}_1\left(\tilde{k}_{r,D,n} R_2\right) - \mathrm{Y}_1\left(\tilde{k}_{r,D,n} R_1\right)\mathrm{J}_1\left(\tilde{k}_{r,D,n} R_2\right)} \tag{7}$$

Here, J_1 is the first order Bessel function of the first kind, and Y_0 and Y_1 are the zeroth and first order Bessel functions of the second kind, respectively. The axial wavenumbers are obtained solving Equation (7) in combination with Equation (6). Details of the solution technique can be found in the work of Selamet *et al.* [14].

Finally, the transversal pressure eigenfunctions in region *D* are given by

$$\psi_{D,n,P}(r) = \begin{cases} \mathrm{J}_0\left(k_{r,D,n} r\right) & 0 \le r \le R_1 \\ F\left(\mathrm{J}_0\left(\tilde{k}_{r,D,n} r\right) - \dfrac{\mathrm{J}_1\left(\tilde{k}_{r,D,n} R_2\right)}{\mathrm{Y}_1\left(\tilde{k}_{r,D,n} R_2\right)} \mathrm{Y}_0\left(\tilde{k}_{r,D,n} r\right) \right) & R_1 \le r \le R_2 \end{cases} \tag{8}$$

with

$$F = \left(\mathrm{J}_0\left(k_{r,D,n} R_1\right) + \frac{\mathrm{j}\tilde{\zeta}_p k_{r,D,n}}{k_0} \mathrm{J}_1\left(k_{r,D,n} R_1\right) \right) \frac{\mathrm{Y}_1\left(\tilde{k}_{r,D,n} R_2\right)}{\mathrm{J}_0\left(\tilde{k}_{r,D,n} R_1\right)\mathrm{Y}_1\left(\tilde{k}_{r,D,n} R_2\right) - \mathrm{J}_1\left(\tilde{k}_{r,D,n} R_2\right)\mathrm{Y}_0\left(\tilde{k}_{r,D,n} R_1\right)} \tag{9}$$

A procedure must be implemented to calculate the unknown coefficients A_n^+, A_n^-, B_n^+, B_n^-, C_n^+, C_n^-, D_n^+, D_n^-, E_n^+, E_n^-, F_n^+, F_n^-, G_n^+ and G_n^-. The standard mode-matching method is considered in this work, which is applied once the proper boundary conditions have been established. At the expansion of the first lateral chamber (left), these conditions are

$$P_A\big|_{z_1=0} = P_B\big|_{z_1=0} \qquad 0 \le r \le R_1 \tag{10}$$

$$U_A\big|_{z_1=0} = U_B\big|_{z_1=0} \quad 0 \le r \le R_1 \qquad U_B\big|_{z_1=0} = 0 \quad R_1 \le r \le R_2 \tag{11}$$

For the contraction of the first lateral chamber (left), the conditions are written as

$$P_B\big|_{z_1=L_B} = P_C\big|_{z_2=0} \qquad 0 \le r \le R_1 \tag{12}$$

$$U_B\big|_{z_1=L_B} = U_C\big|_{z_2=0} \quad 0 \le r \le R_1 \qquad U_B\big|_{z_1=L_B} = 0 \quad R_1 \le r \le R_2 \tag{13}$$

For the expansion of the central dissipative chamber, one has

$$P_C\big|_{z_2=t_{p1}} = P_D\big|_{z_3=0} \qquad 0 \le r \le R_1 \tag{14}$$

$$U_C\big|_{z_2=t_{p1}} = U_D\big|_{z_3=0} \quad 0 \le r \le R_1 \qquad U_D\big|_{z_3=0} = 0 \quad R_1 \le r \le R_2 \tag{15}$$

For the contraction of the central dissipative chamber,

$$P_D\big|_{z_3=L_C} = P_E\big|_{z_4=0} \qquad 0 \le r \le R_1 \tag{16}$$

$$U_D\big|_{z_3=L_C} = U_E\big|_{z_4=0} \quad 0 \le r \le R_1 \qquad U_D\big|_{z_4=L_C} = 0 \quad R_1 \le r \le R_2 \tag{17}$$

At the expansion of the second lateral chamber (right), these are

$$P_E\big|_{z_4=t_{p2}} = P_F\big|_{z_5=0} \qquad 0 \le r \le R_1 \tag{18}$$

$$U_E\big|_{z_4=t_{p2}} = U_F\big|_{z_5=0} \quad 0 \le r \le R_1 \qquad U_F\big|_{z_5=0} = 0 \quad R_1 \le r \le R_2 \tag{19}$$

Finally, for the contraction of the second lateral chamber (right), the conditions are expressed as

$$P_F\big|_{z_5=L_D} = P_G\big|_{z_6=0} \qquad 0 \le r \le R_1 \tag{20}$$

$$U_F\big|_{z_5=L_D} = U_G\big|_{z_6=0} \quad 0 \le r \le R_1 \qquad U_F\big|_{z_5=L_D} = 0 \quad R_1 \le r \le R_2 \tag{21}$$

Equations (10)-(21) are multiplied by proper transversal modes and integrated over the associated cross section. Table 1 presents relevant information regarding the modes considered for each equation and additional data related to the integration.

Table 1 – Mode-matching method. Information about modes and integrals

Condition	Multiplication by	Integration over	
		Duct	Chamber
Pressure Equation (10)	$\psi_{A,s}(r)$	$0 \le r \le R_1$	$0 \le r \le R_1$
Velocity Equation (11)	$\psi_{B,s}(r)$		$0 \le r \le R_2$
Pressure Equation (12)	$\psi_{C,s}(r)$		$0 \le r \le R_1$
Velocity Equation (13)	$\psi_{B,s}(r)$		$0 \le r \le R_2$
Pressure Equation (14)	$\psi_{C,s}(r)$		$0 \le r \le R_1$
Velocity Equation (15)	$\psi_{D,s,P}(r)$		$0 \le r \le R_2$
Pressure Equation (16)	$\psi_{E,s}(r)$		$0 \le r \le R_1$
Velocity Equation (17)	$\psi_{D,s,P}(r)$		$0 \le r \le R_2$
Pressure Equation (18)	$\psi_{E,s}(r)$		$0 \le r \le R_1$
Velocity Equation (19)	$\psi_{F,s}(r)$		$0 \le r \le R_2$
Pressure Equation (20)	$\psi_{G,s}(r)$		$0 \le r \le R_1$
Velocity Equation (21)	$\psi_{F,s}(r)$		$0 \le r \le R_2$

The number of modes is truncated to a suitable value N, and the integrals are evaluated analytically. The acoustic attenuation performance of the muffler is then calculated by means of its transmission loss (TL). The values $A_0^+ = 1$, $A_n^+ = 0$, $n > 0$ (incident plane wave) and $G_n^- = 0$ for n = 0, 1, 2, …. (anechoic termination) are assumed, which yields a system of 12 (N + 1) equations with 12 (N + 1) unknowns (A_n^-, B_n^+, B_n^-, C_n^+, C_n^-, D_n^+, D_n^-, E_n^+, E_n^-, F_n^+, F_n^- and G_n^+). The TL is easily evaluated once the system of equations has been solved.

RESULTS AND DISCUSSION

The geometries considered to validate the proposed method and to analyse the acoustic attenuation performance of the hybrid muffler are detailed in Table 2. In all the cases, the values R_1 = 0.0268 m and R_2 = 0.091875 m are taken into account.

Table 2 – Geometries of hybrid muffler

Geometry	L_B (m)	t_{p1} (m)	L_C (m)	t_{p2} (m)	L_D (m)
1	0.148	0.005	0.148	0	0
2	0.0665	0.005	0.148	0	0
3	0.05	0.001	0.148	0.001	0.01
4	0.05	0.001	0.148	0.001	0.05

Geometries 1 and 2 are considered for comparison with experimental measurements as well as finite element calculations. The porosity of the perforated passage in the experimental prototypes is very high (over 80%), and therefore the value $\tilde{\zeta}_p = 0$ is considered in the calculations. The absorbing material (texturized Advantex fiber glass roving from Owens Corning) is defined by the following formulae for the wavenumber $\tilde{k}$ and characteristic impedance $\tilde{Z}$

$$\tilde{k} = k_0\left[\left(1+0.16\left(f\,\rho_0/R\right)^{-0.577}\right)+\mathrm{j}\left(-0.18897\left(f\,\rho_0/R\right)^{-0.595}\right)\right] \tag{22}$$

$$\tilde{Z} = Z_0\left[\left(1+0.09534\left(f\,\rho_0/R\right)^{-0.754}\right)+\mathrm{j}\left(-0.08504\left(f\,\rho_0/R\right)^{-0.732}\right)\right] \tag{23}$$

where f is the frequency and R is the steady airflow resistivity: 4896 rayl/m or 17378 rayl/m for bulk densities of 100 kg/m^3 or 200 kg/m^3, respectively [12]. Figure 2 shows the validation of the proposed procedure: the transmission loss of geometries 1 and 2 for R = 4896 rayl/m, calculated from analytical and FEM results, exhibits an excellent agreement. In addition, experimental measurements are also included, showing the accuracy of the models for practical applications. In the case of geometry 2, the length L_B is short enough to provide an attenuation peak that appears close to 1600 Hz, and improves the acoustic behaviour in comparison with geometry 1 in the mid frequency range. At high frequencies, the attenuation depends mainly on the central dissipative chamber, and therefore both geometries exhibit similar transmission loss levels.

Figure 3 shows the attenuation of geometry 3, as well as the transmission loss its components considered separately, that is, the left and right lateral resonators and the central dissipative chamber. The lengths L_B and L_D are chosen to provide two resonant peaks that improve the performance of geometry 3 in comparison with the central dissipative chamber in a wide frequency range. The frequencies of the peaks in the hybrid muffler can be predicted easily since they are very similar to those associated with the resonators considered independently. For low frequencies, a detrimental effect is found for the hybrid configuration in comparison with the central dissipative chamber. At high frequencies, the acoustic performance is almost similar.

The effect of the resistivity and the presence of a perforated pipe (defined by the porosity σ = 11%, thickness t_p = 0.001 m and hole diameter d_h = 0.0035 m [14]) is presented in Figure 4 for geometry 4. Since the current configuration involves equal

lengths for both lateral chambers ($L_B = L_D = 0.05$ m) a single peak is found in the *TL* curve, with an attenuation level higher than this depicted in the previous figure for geometry 3. The attenuation peak does not exhibit any significant modification for variations of resistivity or the presence of the perforated pipe. At high frequencies, an increase in the resistivity of the absorbing material leads to a slightly higher attenuation level in the absence of the perforated pipe. When the presence of the perforated central passage is included in the calculations, the effect of the resistivity is almost negligible.

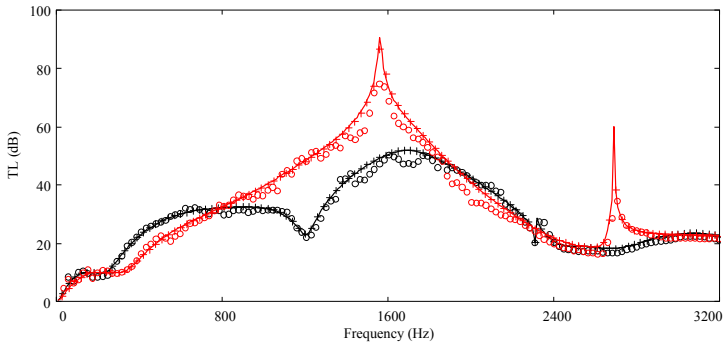

Figure 2 – TL of hybrid muffler: ooo, *geometry 1, experimental;* ——, *same, analytical;* +++, *same, FEM;* ooo, *geometry 2, experimental;* ——, *same, analytical;* +++, *same, FEM.*

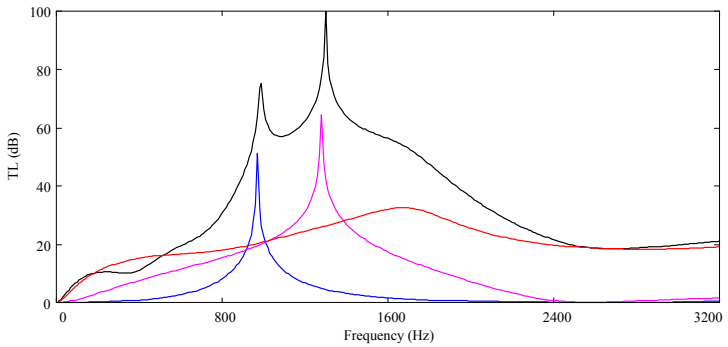

Figure 3 – TL of hybrid muffler (geometry 3) and components: ——, *geometry 3;* ——, *central dissipative chamber;* ——, *left resonator;* ——, *right resonator.*

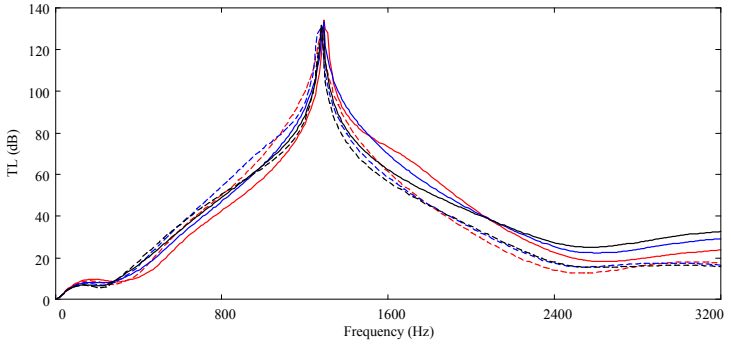

Figure 4 – TL of hybrid muffler (geometry 4): ——, *without perforate, R = 4896 rayl/m;* ——, *same, R = 10000 rayl/m;* ——, *same, R = 17378 rayl/m;* – – –, *with perforate, R = 4896 rayl/m;* – – –, *same, R = 10000 rayl/m;* – – –, *same, R = 17378 rayl/m.*

CONCLUSIONS

The acoustic attenuation performance of circular hybrid mufflers has been analysed by means of a two-dimensional axisymmetric analytical approach based on the mode-matching method. The hybrid configuration consists of two lateral resonators and a central dissipative chamber. The attenuation exhibits the desirable effect of transversal resonances in the lateral chambers, providing a considerable noise reduction at selected frequencies, and dissipation in the absorbing material, leading to the suppression of high frequency noise.

ACKNOWLEDGEMENTS

Financial support of Ministerio de Ciencia y Tecnología (project DPI2003-07153-C02-01), Conselleria d'Empresa, Universitat i Ciència (grant Grupos 04/63) and Universidad Politécnica de Valencia is gratefully acknowledged. The authors wish also to thank Dr. N. T. Huff and Mr. A. Reinartz, from Owens Corning, for providing the texturized Advantex fiber glass roving.

REFERENCES

[1] Cummings, A., Chang, I. J., "Sound attenuation of a finite length dissipative flow duct silencer with internal mean flow in the absorbent", Journal of Sound and Vibration, **127**, 1-17 (1988).
[2] Delany, M. E., Bazley, E. N., "Acoustical properties of fibrous absorbent materials", Applied Acoustics, **3**, 105-116 (1970).
[3] Denia, F. D., Albelda, J., Fuenmayor, F. J., Torregrosa, A. J., "Acoustic behaviour of elliptical chamber mufflers", Journal of Sound and Vibration, **241**, 401-421 (2001).
[4] Denia, F. D., Selamet, A., Fuenmayor, F. J., Kirby, R., "Sound attenuation in partially-filled perforated dissipative mufflers with extended inlet/outlet", Proceedings of the 12th International Congress on Sound and Vibration. (Lisbon, Portugal, 2005).
[5] Ji, Z. L., "Boundary element analysis of a straight-through hybrid silencer", Journal of Sound and Vibration, **292**, 415-423 (2006).
[6] Kirby, R., "Simplified techniques for predicting the transmission loss of a circular dissipative silencer", Journal of Sound and Vibration, **243**, 403-426 (2001).
[7] Kirby, R., "Transmission loss predictions for dissipative silencers of arbitrary cross section in the presence of mean flow", Journal of the Acoustical Society of America, **114**, 200-209 (2003).
[8] Munjal, M. L., *Acoustics of Ducts and Mufflers*. (Wiley-Interscience, New York, 1987).
[9] Peat, K. S., Rathi, K. L., "A finite element analysis of the convected acoustic wave motion in dissipative silencers", Journal of Sound and Vibration, **184**, 529-545 (1995).
[10] Selamet, A., Denia, F. D., "Acoustic behavior of short elliptical chambers with end central inlet and end offset or side outlet", Journal of Sound and Vibration, **245**, 953-959 (2001).
[11] Selamet, A., Ji, Z. L., Radavich, P. M., "Acoustic attenuation performance of circular expansion chambers with offset inlet/outlet: II. Comparison with experimental and computational studies", Journal of Sound and Vibration, **213**, 619-641 (1998).
[12] Selamet, A., Lee, I. J., Huff, N. T., "Acoustic attenuation of hybrid silencers", Journal of Sound and Vibration**, 262**, 509-527 (2003).
[13] Selamet, A., Radavich, P. M., "The effect of length on the acoustic attenuation performance of concentric expansion chambers: An analytical, computational and experimental investigation", Journal of Sound and Vibration, **201**, 407-426 (1997).
[14] Selamet, A., Xu, M. B., Lee, I. J., Huff, N. T., "Analytical approach for sound attenuation in perforated dissipative silencers", Journal of the Acoustical Society of America**, 115**, 2091-2099 (2004).